Collective low-frequency excitations in a molecular glass

1994 J. Phys.: Condens. Matter 6 405

(http://iopscience.iop.org/0953-8984/6/2/012)

J. Phys.: Condens. Matter 6 (1994) 405–420. Printed in the UK

Collective low-frequency excitations in a molecular glass

F J Bermejo†, A Criado‡, M García-Hernández†, J Alonso§, C Prieto¶ and J L Martínez*+

† Instituto de Estructura de la Materia, Consejo Superior de Investigaciones Cientificas, Serrano 123, E-28006 Madrid, Spain

‡ Departamento de Física de la Materia Condensada, Universidad de Sevilla and Instituto de Ciencia de Materiales, PO Box 1065, E-41080 Sevilla, Spain

§ Rutherford Appleton Laboratory, Chilton, Didcot, Oxon OX11 0QX, UK

¶ Instituto de Ciencia de Materiales, Departamento Física-Aplicada C-IV, Facultad de Ciencias, Universidad Autónoma de Madrid, E-28049, Spain

* Institut Laue–Langevin, 156X, F-38042 Grenoble Cédex, France

Received 30 June 1993, in final form 22 September 1993

Abstract. The collective dynamics of an organic molecular glass former has been investigated by means of coherent inelastic scattering of neutrons at several temperatures below the glass transition. The excitations observed by means of the inelastic neutron scattering response are characterized by the wavevector dependences of their average frequencies. The inelastic spectra are analysed on the basis of a lattice dynamics calculation for the polycrystalline reference state as well as a molecular dynamics simulation of a computer-generated glass. The excitation frequencies are discussed in terms of average ω_m quantities, defined as the peak maxima of the longitudinal current–current autocorrelation function. An assessment of the reliability of the simulation results is finally made by comparison with the experimentally accessible magnitudes.

1. Introduction

The understanding of the collective dynamical properties of glasses at intermediate temperatures still constitutes an open question in condensed matter physics. Recent theoretical advances, of both a phenomenological origin [1, 2] and a semi-microscopic nature [3], have made significant progress towards providing us with an understanding of static thermal and heat transport anomalies in disordered systems in terms of the scattering of long-wavelength (low-frequency) excitations by localized entities.

However, most of the available experimental data concerning the propagation characteristics of low-frequency excitations in glasses concern the hydrodynamic limit, where such phenomena are probed by optical, thermal, acoustical or dielectric spectroscopies [4, 5]. A study at wavevectors well within the kinetic regime accessible to neutron spectroscopy (i.e. reciprocal wavevectors comparable with the interparticle separations), has been hindered by the fact that the most heavily studied systems, such as metallic, silica or chalcogenide glasses, show relatively high elastic constants; this fact introduces considerable difficulties for the study of these excitations at wavevectors within what can be considered to be the analogue of the first Brillouin zone (i.e. for momentum transfers below $Q_p/2$, where Q_p is the position of the main diffraction peak). Such difficulties are caused by kinematical restrictions imposed by the high incident energies required to study the spectra in the energy-loss side, where these excitations become clearly visible.

+ Permanent address: Instituto de Ciencia de Materiales, Departamento Física-Aplicada C-IV, Facultad de Ciencias, Universidad Autónoma de Madrid, E-28049, Spain.

0953-8984/94/020405+16$07.50

The purpose of this paper is to present a comparison of experimental and computer simulation results regarding the collective dynamics of an organic glass former (methanol) for which the single-particle dynamics† [6] and the anomalies in the specific heat [7] as well as some preliminary accounts of the experimental work [8, 9] have already been studied (note that a full account of the adiabatic calorimetric results for this sample from 5–200 K for its liquid, glass and polycrystalline solid phases is contained in [7]). The chosen sample, due to the small size of the molecular unit and to the moderate adiabatic sound velocity, constitutes an adequate choice in order to perform a concurrent study by means of a computer simulation using molecular dynamics (MD) for the glass and lattice dynamics (LD) for its polycrystalline counterpart, as well as inelastic neutron scattering (INS).

The outline of the paper is as follows. Section 2 presents some brief details concerning the experimental and calculational approaches; the main results are given in section 3; a discussion of results and a comparison of experimental and simulated quantities is given in section 4; and the main conclusions are enumerated in section 5.

2. Experimental and computational details

The glass samples were prepared by rapid quenching of the room-temperature liquid (fully deuterated methanol CD_3OD) in a liquid nitrogen bath. The thermodynamic glass transition temperature T_g was located as a rather broad feature covering a temperature range $106\,K < T < 113\,K$ showing a strong dependence on the cooling rates and sample environment conditions‡, and a supercooled liquid phase is formed after subsequent heating. At least three crystalline modifications exist between the crystallization temperature $T_{cr} = 130\,K$ and the melting $T_m = 175\,K$, of which two have been studied in detail for a fully hydrogenated sample [10].

The inelastic neutron scattering experiments were performed using the IN6 time-of-flight and the IN8 triple-axis spectrometers, both located at the Institut Laue Langevin, Grenoble, France, and the relevant experimental details for the latter set of experiments have already been given [8, 9]. The high-energy-resolution experiments were carried out on the above-mentioned time-of-flight spectrometer using an incident wavelength of 5.12 Å and a plate sample of 6 mm thickness composed of aluminium foils separated by horizontal cadmium coated spacers every millimetre in the vertical direction was used (see [8] and references therein). Absorption corrections, conversion of the cross section data into dynamical structure factors and interpolation into constant Q followed the same procedures as described in [6]. The multiple-scattering correction was evaluated using one of the volume elements of the sample holder (33 mm length × 6 mm width × 1 mm height) using the DISCUS code [11] using the MD spectra as single-scattering kernels. Because of the relatively low temperatures explored in this work (10–60 K) no multiphonon corrections were deemed necessary.

2.1. Computational details

The details concerning the computer calculations regarding both the glass and normal liquid phases [6, 7, 12] have already been given, and therefore only the validation of the model potential regarding the prediction of collective dynamical properties is described in some detail.

† Terahertz (THz) frequency units are used since they constitute a natural choice for relatively high-energy inelastic spectrum analysis. Those used in [6] are millielectronvolts (meV) because of the low energy transfers involved. The conversion factors are $1\,THz = 4.1357\,meV = 33.36\,cm^{-1}$.

‡ Preliminary measurements of the dielectric response have shown a strong frequency dependence of T_g. A systematic increase of T_g with the sample volume was also noticed.

The model potential used in both LD and MD calculations was able to reproduce the observed crystal structure [13] to a rather good degree of accuracy (the maximum percentage deviation of the cell parameters after energy minimization with respect to atomic positions was 3.8). To assess the reliability of the potential model to predict collective dynamical properties, the observed lattice frequencies measured by means of Raman and far-infrared spectroscopies [14] were compared with the frequencies of the main spectral features appearing in the $Z(\omega)$ density of vibrational states given in previous work [6, 7], and the results are given in table 1. From a comparison of the lattice frequencies measured by optical spectroscopic means at temperatures where the harmonic approximation should hold (20 K), with those arising from the LD calculation, it can be seen that the latter reproduces acceptably well the experimental observations. Since no detailed mode assignment is available, the comparison must be of a qualitative nature. The maximum difference between the observed and calculated frequencies is about 0.1 THz (i.e. $3.33\,cm^{-1}$), which is close to the estimated uncertainties quoted in [14] (about $1\,cm^{-1}$ for strong well isolated peaks, and $3\,cm^{-1}$ for shoulders or broad features).

Table 1. A comparison of experimental and calculated lattice frequencies for CD_3OD. The symbols denote peak intensities as follows: strong (st), shoulder (sh), medium (m), weak (w), and combinations of these.

Raman (20 K)	IR (20 K)	LD (harmonic)	Raman (20 K)	IR (20 K)	LD (harmonic)
		1.38 st	4.84 w	4.92 st	4.88 st
1.51 mst		1.58 sh			5.20st
		1.62 st			5.87 st
1.80 mw	1.97 mw	1.89 st		6.35 mst	6.23 st
2.22 mw	2.17 mw	2.13 sh			6.63 st
2.43 mst		2.29 m		6.94 sh	7.19st
		2.53 st			7.82st
2.64 sh	2.68 sh	2.77 sh		8.11 mst	8.10 st
3.06 sh	3.04 sh	2.89 st			9.46 st
		3.20 st			9.06 st
3.48 w	3.40 sh	3.40 st			9.65 st
3.87 mst	3.93 mst	4.00 sh		10.07 mst	
		4.28 st			10.66 st
4.41 w		4.56 sh			11.08 st
					11.38 st

The strong anharmonic effects which become noticeable above 20 K are expected to manifest themselves as frequency shifts relative to their harmonic reference value, as well as a noticeable broadening of the individual phonon lines due to finite-lifetime effects brought in by the multiphonon interactions. The interparticle potential model can therefore be considered as a reliable one for the kind of study herein pursued. The absence of IR or Raman data concerning the high-temperature crystal precludes a comparison of the crystal LD or MD results along the same lines followed for the low-temperature case.

3. Results

3.1. Experimental results

3.1.1. Low incident energy. The main purpose of this series of experiments was to clarify the origin of a low-frequency component whose presence was noticed during the preliminary analysis of triple-axis spectra [8]. The time-of-flight spectra were found to exhibit a finite-frequency feature, located at considerably lower frequencies than the ones observed for the

polycrystal, which, once transformed into constant Q, led to a noticeable dependence of the peak maxima with the wavevector [9]. However, because of kinematical restrictions, only momentum transfers about Q_p were explored, thus making difficult the assignment of the observed excitations. A subsequent study on a mostly incoherent scattering sample [7] now enables the identification of this low-frequency component with the one observed in the spectra of the latter samples, a feature which is characteristic of a large number of glasses and which is postulated as one of the universal signatures of the glassy state. Some representative constant-Q spectra are depicted in figure 1 as neutron-weighted current–current autocorrelations (i.e. $J_{N,I}(Q,\omega) = \omega^2 S(Q,\omega)/Q^2$) in order to eliminate as much as possible the contamination from the resolution-broadened elastic line.

As shown in the graphs displayed in figure 1, the frequency distribution of the inelastic intensity seems to follow two different regimes below and above 10 K respectively. At the lower (5 K and 10 K) temperatures the low-frequency peak appears displaced to very low frequencies, although it moves up to about $\simeq$ 0.5 THz once the spectra are corrected by the Bose factor. The peak which becomes clearly visible at 10 K centred at about 3.5 THz (at 5 K the statistics is too poor to separate it from the background noise) corresponds to rotations of the methyl group, as was evidenced in [7]. The spectra corresponding to the higher-temperature glass phase (35 K and above), show a well defined maximum located at somewhat less than 1 THz, not showing any strong temperature dependence, which corresponds to the excitation observed in a previous work [6] for an incoherently scattering sample at 0.5 THz, once the frequency upshift caused by the multiplication by ω^2 is accounted for. On the other hand, the spectrum for a polycrystalline sample ($T = 135$ K) is evidence for the lack of any clear finite-frequency peak below the main one located at 1.4 THz, which arises from intense rotational peaks superimposed to the sonic modes, as was shown in [6] from an analysis of the mode eigenvectors derived in the LD calculation. Only broad and structureless features appear in the normal liquid ($T = 200$ K), although the overall shape of the spectrum closely resembles that of the high-temperature glass.

As shown from the analysis of an incoherent scattering sample [6], this low-frequency inelastic feature can be identified with the excess of vibrational modes clearly visible by comparison of the low-frequency tails of the generalized $Z(\omega)$ vibrational densities of states of a glass and its polycrystalline counterpart. Such an excess of low-frequency modes has also been shown to lead to the appearance of a noticeable hump in the C/T^3 specific heat curves [7] which occurs at temperatures substantially lower than those where a similar feature also shows up in calorimetric measurements of the polycrystalline form [7].

3.1.2. High incident energy. As expected, only rather structureless features due to resolution-broadening effects can be seen in the coherent INS triple-axis spectra (TAS) of the glassy sample at all the explored temperatures, and an example of the measured spectra is given in figure 2. An inelastic response is readily apparent at the two lowest wavevectors, which show a feature on the neutron energy-loss side of the spectrum located at frequencies of about 2.5 THz.

To analyse the TAS spectral intensities, a contribution with the form of a damped harmonic oscillator was used in previous work [8] in order to account for the envelope of finite-frequency excitations. Such an spectral component is given by

$$S_{\mathrm{exc}}(Q,\omega) = H(Q)/\pi(n(E)+1)\frac{4\omega\omega_q\Gamma_q}{[\omega^2-(\omega_q^2+\Gamma_q^2)]^2+4\omega^2\Gamma_q^2} \qquad (1)$$

where $H(Q)$ is an amplitude factor (i.e. one-phonon structure factor) which was left as a free parameter, $n(E)$ is a Bose factor, ω_q represents here the bare excitation frequencies

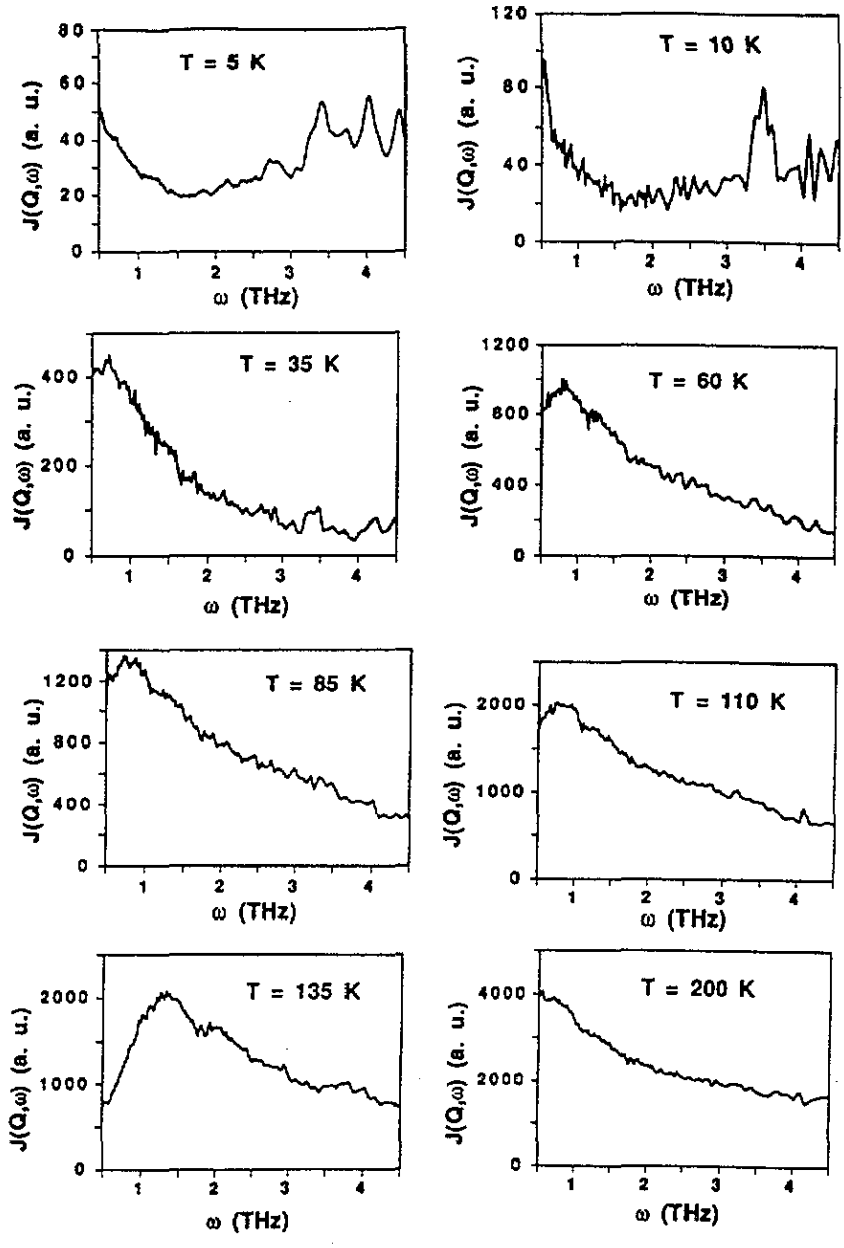

Figure 1. Constant-Q energy-gain $J_{N,I}(Q,\omega)$ current–current spectra for glassy CD_3OD samples for eight temperatures covering the glass stability phase. The curves correspond to experimental spectra generated by interpolations on the constant-angle $S(\Theta,\omega)$ surface performed using the INGRID code. All spectra correspond to $Q = 2.1\,\text{Å}^{-1}$, chosen in order to span a large dynamic range.

and Γ_q accounts for the linewidth parameter required to reproduce the observed lineshape. Since, as will be illustrated below, a rather large portion of the linewidth comes from the broad distribution of excitation frequencies caused by the topological disorder, this implies that this parameter will contain contributions from both homogeneous broadening, due to

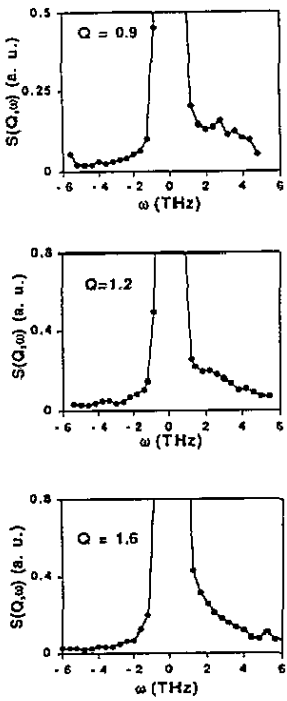

Figure 2. A representative sample of the measured high-incident-energy spectra for three different values of momentum transfer. The spectra correspond to a temperature of 60 K. The full curves are interpolations using spline functions, and are given as a guide to the eye.

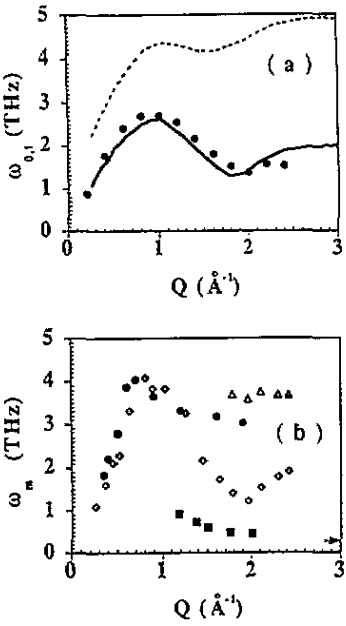

Figure 3. (*a*) The reduced ω_0 second (full curve) and fourth ω_l (broken curve) frequency moments of the MD simulated glass. The full circles show the second moment corresponding to the polycrystalline solid. (*b*) The ω_m average frequencies derived from fits of the neutron inelastic intensities (full circles) and from peak positions of the different structures appearing in the current–current correlation function calculated from the MD simulation (open lozenges and triangles). The full squares show the dispersion of the low-frequency peak shown in the low-incident-energy experiments, and the arrow marks the limiting (single-particle) frequency of this low-energy peak.

the damping of the individual modes, and inhomogeneous broadening due to the spread in frequency of the glass excitations.

The model scattering law used to analyse the experimental intensities was, at that time, considered to be a sum of a zero-frequency (quasielastic) response and the $S_{exc}(Q,\omega)$ inelastic contribution. Although, as a result of the data presented in this work, the quasielastic response should be substituted by a low-frequency (0.5 THz) component, a model scattering law encompassing these two components as well as the elastic response (a delta function at zero energy-transfer), seems to be the only realistic approach to analysing the experimental data.

The parameter values corresponding to the experimental functions were taken to be the same than those given in [8]. Once these functions were calculated, the position of the main peak of $J_{N,I}(Q,\omega)$, ω_m, was estimated, and the results are shown in figure 3. The ω_m frequencies plotted in the figure are shifted towards somewhat higher values than the renormalized excitation frequencies shown in figure 2 of [8], since the large linewidth required to reproduce the mode envelopes causes such a shift once the structure factors are multiplied by the frequency squared. A comparison with the first two (non-zero) even-order

moments of the dynamical structure factor as calculated from MD is also shown in the figure. As can also be seen, the frequencies corresponding to the ω_m peak maxima derived from the low-incident-energy experiment show a weak dependence on momentum transfer, and at large Q approach the frequency observed in the previous study.

As will be shown below, additional intensity at higher frequencies arising from optical manifolds will make the approximation of only one inelastic component rather inadequate for representing the simulation data. However, the analysis of the experimental data in terms of more than one or two components is precluded by the achievable statistical accuracy and the limited number of data points in energy transfers measurable using conventional triple-axis spectroscopy.

3.2. Molecular and lattice dynamics results

The short-range structure (below 10 Å) of the glassy and polycrystalline phases is compared in figure 4; this shows the static $g_{\alpha\beta}(r)$ partial pair correlation functions for the six different combinations of atom types which, once weighted by the appropriate factors, give after Fourier transformation an $S(Q)$ static structure factor which can be compared favourably with experiment [15]. As can be seen from the figure, the structure corresponding to the main features appearing in the glass phase has a polycrystalline correlate, except perhaps for some sharp features such as the double peak at about 4.8 Å in $g_{DD}(r)$ and the intense peak at 3.2 Å in the $g_{CD}(r)$ function.

From the dispersion curves calculated by means of the LD code, estimates of the sound velocity in the crystalline solid have been made and an average sound velocity was estimated in order to characterize the elastic behaviour of the polycrystal. A mean speed of sound of $2716\,\mathrm{m\,s^{-1}}$ was calculated as a spherical average over the six higher-symmetry directions of the single crystal, and the average of the elastic moduli following the prescription given by Bathia and Singh [17] (see also Hirth and Lothe [17]) gives a value of $9.68 \times 10^9\,\mathrm{N\,m^{-2}}$, a value significantly higher than the one derived for the low-temperature glass from an analysis of the light-scattering spectra (a preliminary account of Brillouin scattering for the liquid phase has already been given in [16]; the value for the velocity of sound measured in a recent experiment was $2512\,\mathrm{m\,s^{-1}}$, and estimates for the longitudinal moduli in both glass and liquid phases were $M_\infty = 7.94\times10^9\,\mathrm{N\,m^{-2}}$ for the glass at 60 K and $M_\infty = 2.14\times10^9\,\mathrm{N\,m^{-2}}$ for the liquid at 200 K).

A representative sample of the $S(Q,\omega)$ calculated for the glass phase from an analysis of the MD trajectories (the elastic peak, i.e. $I(Q,t=\infty)$ was subtracted before the transformation into frequency space in order to avoid termination ripples) as well as the associated $J_{N,l}(Q,\omega)$ longitudinal current–current autocorrelation functions is depicted in figure 5. From inspection of the figure it can be seen that clearly defined excitations seem to exist within a limited range of momentum transfers, for which an upper bound can be set at $Q \simeq 0.9\,\mathrm{Å^{-1}}$. On the other hand, substantial inelastic intensities start to build up at higher frequencies and wavevectors, giving rise to rather broad features which, as expected, approach the $Z(\omega)$ density of states at the largest explored Q values. Apart from the well defined peak at about 7 THz, which becomes very intense as the single-particle limit is approached and which was assigned as arising from mostly rotational motions, a broad structure centred at about 3.5 THz and a large manifold of acoustic and low-frequency optical branches is apparent for frequencies below 1.5 THz.

The $S(Q,\omega)$ dynamic structure factors calculated from an analysis of the MD results were compared with the same quantity regarding the polycrystal. For such a purpose, and in order to facilitate the comparison, the polycrystalline $S(Q,\omega)$ were smoothed using a binning procedure to remove the delta-like character of the calculated spectra. An example

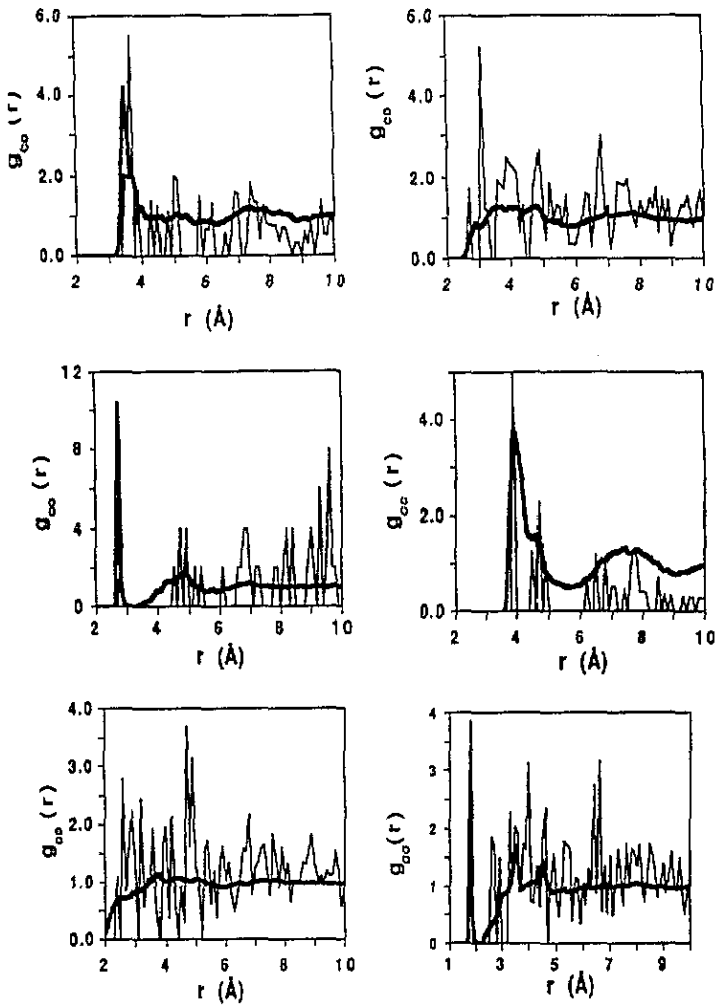

Figure 4. A comparison of the $g_{\alpha\beta}$ static pair correlation functions calculated for the computer-generated glass (thick curve), and from the evaluation of the atomic contacts by means of orientational averages corresponding to the polycrystalline LD calculation (thin curve).

of such a comparison for selected values of momentum transfers is shown in figure 6. The most remarkable facts arising from this comparison are the following.

(i) The spectral intensity at frequencies below 1 THz is consistently higher in the glass case than in the crystal. A well defined peak develops within this frequency range and becomes more noticeable at momentum transfers of about $Q_p/2$ and greater, where most of the spectral intensity is transferred to higher optical manifolds.

(ii) The lineshapes of the spectra corresponding to the two states seem to get closer as the hydrodynamic regime is approached. In fact, the line profile of the lowest explored wavevector in the MD simulation ($Q \simeq 0.26\,\text{Å}^{-1}$) can be reproduced, except for the low-frequency tail, using polycrystalline data shifted to lower frequencies.

(iii) For relatively large wavevectors (i.e. $Q > 2.0\,\text{Å}^{-1}$), both spectra have a similar shape, although the main peaks in the glass spectra are located at frequencies of about 0.5 THz, whereas a far larger frequency shift is apparent for the polycrystal. Also, the

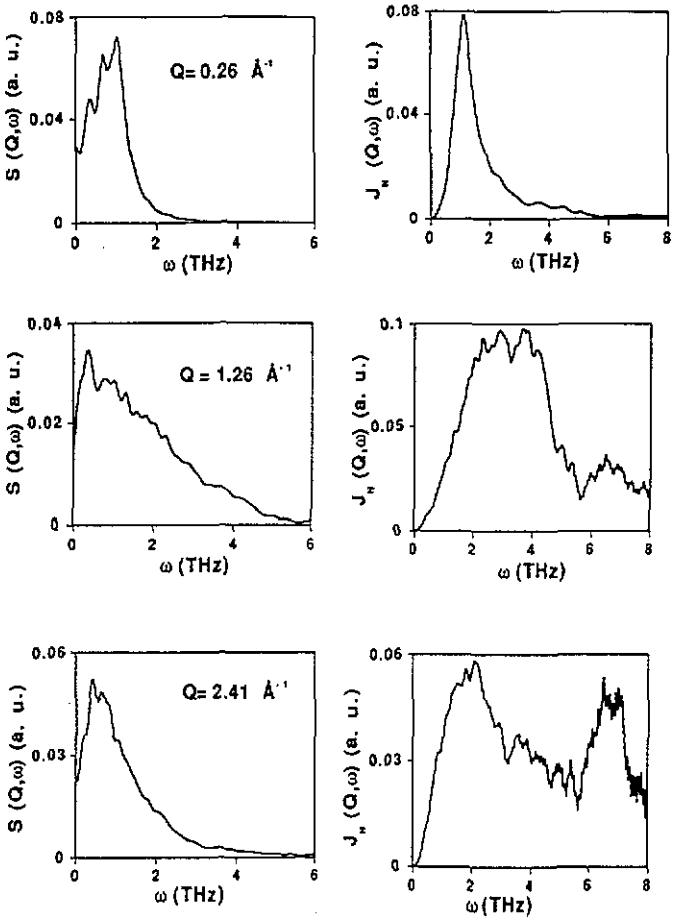

Figure 5. Calculated $S(Q,\omega)$ dynamic structure factors (left column) and the associated $J_{N,I}(Q,\omega)$ *current–current correlation functions from the* MD *simulation results (right column),* for several representative values of the momentum transfer.

high-frequency tail of the glass decays in a smoother fashion than that of the polycrystal case.

The ω_m frequencies corresponding to the location in frequency of the most prominent peaks appearing below 5 THz in the current–current autocorrelation functions $J_{N,I}(Q,\omega)$ *calculated from the simulation data were shown in figure 3. The high-frequency mode at* 7 THz does not show any noticeable wavevector dependence within the range of momentum transfers where it is clearly visible, and the same qualifications apply to the component located at about 3.7 THz. The origin of this latter band was found in a previous paper, where it was seen that such a feature which starts to develop at about 0.4 $Å^{-1}$ becomes the dominant spectral feature at about $Q_p/2$ and continues as a well resolved peak towards the single-particle limit. In fact, the analysis of the mode eigenvectors corresponding to a well resolved peak appearing at the same frequency in the LD calculation revealed that these modes are of a mixed rotational–translational character, with moduli of the translational and rotational vector components amounting to nearly 0.5 in both cases. The higher-lying mode envelope was shown in a previous paper [6] to be dominated by the rotational components

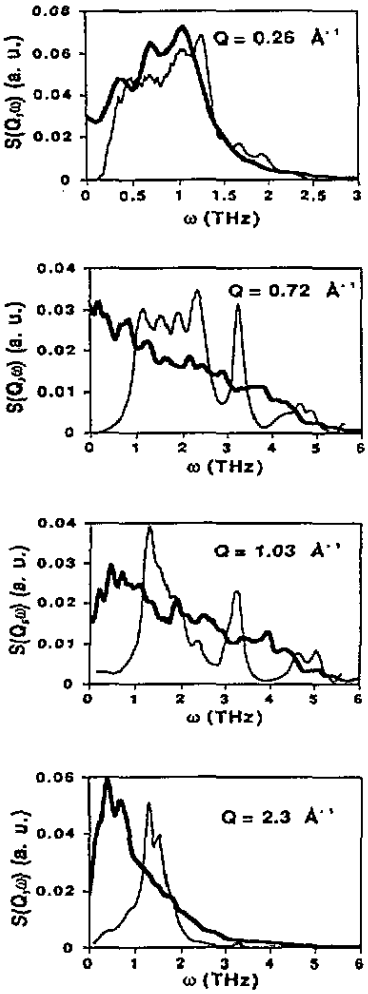

Figure 6. A comparison between the $S(Q, \omega)$ dynamic structure factors of the computer generated glass (thick curve) and those calculated for the polycrystal (thin curve). In order to facilitate the comparison the polycrystal data were broadened by means of binning into groups of twenty frequency channels.

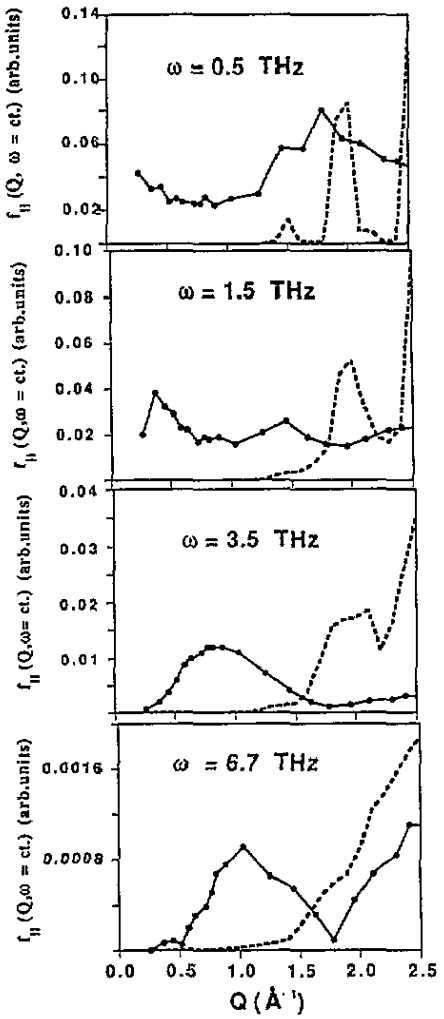

Figure 7. Wavevector dependence of the intensities of the functions $f_{\parallel}(Q, \omega)$ for selected values of the energy transfers as shown. The full circles and curves are the glass intensities, and the broken curves represent the polycrystal data.

of the molecular hydrogens, and the corresponding excitation in the crystalline phase was found to exhibit a rather localized behaviour.

Below $0.8\,\text{Å}^{-1}$ the agreement between the ω_m frequencies derived from experimental and MD means is remarkable. Furthermore, the agreement between the sound velocities quoted in [8] from an analysis of the lower-temperature spectra ($2482(30)\,\text{m s}^{-1}$), with that calculated for the computer-generated glass ($2750(250)\,\text{m s}^{-1}$), and the light-scattering result of $2512\,\text{m s}^{-1}$ can be considered as reasonably good, once one takes into account the uncertainties in the extrapolation procedures (to zero momentum transfer in the neutron case) as well as the statistical accuracy of the data.

As is also shown in figure 3, the second reduced-frequency moments ω_0 calculated for

the glass and polycrystal show similar features, although the crystal data are consistently displaced towards higher frequencies and a small mismatch of the relative phases of the oscillations occurs as a consequence of a shift in the maxima of the structure factor of the crystalline phase. The ω_t fourth frequency moment shows a smoother behaviour, and from $Q = 3\,\text{Å}^{-1}$ reaches a nearly constant value of 4.9 THz. Higher-order moments show, as expected, less marked structure.

As an additional test, the dependence of the $f_{\|}(Q,\omega)$ inelastic intensity functions on momentum transfer, for selected values of the energy transfer for the simulated glass, is shown in figure 7. Such quantities which are defined through [18, 19]

$$S(Q,\omega) = \mathrm{e}^{2W(Q)}\frac{\hbar Q^2}{2M_{\text{mol}}}\left(2\omega\sinh(\omega\beta)\right)^{-1} f_{\|}(Q,\omega) \tag{2}$$

$$\int_0^\infty \mathrm{d}\omega\, f_{\|}(Q,\omega) = 1 \tag{3}$$

in order to remove the trivial Q^2 dependence, can be interpreted as inelastic structure factors [20], and have been used successfully in the analysis of the INS spectra of glasses showing strong short-range correlations (i.e. vitreous silica), and can constitute a basis for proposing a model of the microscopic dynamics. For such a purpose, constant-ω spectra, corresponding to energies which correspond to local maxima in the $Z(\omega)$ densities of states, were calculated from the MD simulation and LD data.

As can be seen from the data shown in figure 7, several noticeable differences between the two constant-frequency spectra are clearly seen. At the lowest-energy transfer (0.5 THz) which corresponds to the low-frequency peak characteristic of the glass phase, both polycrystal and glass spectra show a pronounced feature which basically corresponds to a prolongation of the peaks seen in the $S(Q)$ static structure factors at Q_p. A strong increase in intensity as Q is decreased from $0.5\,\text{Å}^{-1}$ is also visible in the glass spectra, although the precise location of its maxima is precluded by the finite-size nature of the MD simulation. At larger energy transfers (1.5 THz) similar phenomena appear, although the peak at Q_p is now severely depleted and the strong increase in intensity at low Q in the former case gives rise to a small peak at $\sim 0.35\,\text{Å}^{-1}$ which moves to larger wavevectors as the energy transfer is increased. The qualitative behaviour of the constant-ω spectra at energy transfers of 3.5 THz and 6.7 THz show that a well defined broad maximum appears near $Q_p/2$, and a second maximum starts to develop in the spectra corresponding to the highest energy transfer. The origin of such features is discussed in the next section.

4. Discussion

In what follows, some comparisons between the simulated and experimental data as well as the main differences between the calculated magnitudes for the glass and polycrystal are discussed.

4.1. Static structure

From a comparison of the static $g(r)$ partial pair correlations shown in figure 4, it can be seen that the most noticeable differences in the short-range geometrical arrangements of the two systems are those corresponding to correlations with a stronger 'orientational' character (i.e. $g_{\text{OD}}(r)$, $g_{\text{DD}}(r)$), thus indicating the lack of linearity in the hydrogen-bonded chains present in the glass phase. From a consideration of the experimental functions for a low-temperature

glass [15] or from the simulated $g(r)$ function for the molecular centre of mass [6], a lower bound for the coherence length of ~ 20 Å can be set, something which at first sight would imply that the most important differences in the dynamical behaviour of the glass and polycrystal should be sought at wavevectors smaller than ~ 0.3 Å^{-1}, barely reachable by simulational or neutron scattering means. As evidenced in the comparison of $g(r)$ functions corresponding to heavy-atom contacts (carbon and oxygen) for glass and crystalline states, the rather smooth behaviour of the glass correlations should be better ascribed to a dense distribution of atomic contacts rather than to an inherent thermal broadening of the individual delta-like components defining the $g(r)$, since at the relatively low temperatures where the simulation was carried out (35 K), the mean-square displacements for these atoms never exceed 0.03 Å^2.

4.2. Inelastic structure factors

Even if the modulus of the wavevector Q cannot be considered to be a good 'quantum number', the wavevector dependence of the intensities of the functions $f_{\|}(Q,\omega)$ shown in figure 7 reveals some features which are common to other studies on glassy dynamics carried out by simulational means on idealized (Lennard-Jones spheres) systems [18, 19]. In particular, the strong rise towards $\lim_{Q\to 0}$ at low energy transfers unveils the presence of sonic excitations with wavelengths larger than the simulation box (a cube of side ~ 24 Å). The origin of the latter feature, as well as the well defined maximum appearing at about $Q_p/2$ at larger transfers, can be easily visualized as follows. At low Q values where the $S(Q) = \int d\omega\, S(Q,\omega)$ only shows rather shallow features, the spectral power is distributed in a narrow frequency range so that in order to keep the frequency integral over $f_{\|}(Q,\omega)$ constant, relatively high values of the intensity at low energy transfers are required. Because of the steep increase in spectral width up to $Q_p/2$ [8], as evidenced by the present results as well as previous experimental data (see figure 2(*b*) of [8]), for energy transfers not far from the low-frequency maxima in $S(Q,\omega)$, the height of these functions with decreasing Q should show a pronounced rise. On the other hand, as the energy transfer is increased, most of the inelastic intensity from low-Q spectra will become very small, and since the width of $S(Q,\omega)$ goes through a maximum at about $Q_p/2$ and a local minimum at Q_p (see figure 6 for MD and figure 2(*b*) of [8] for experiment), a maximum in the intensity $f_{\|}(Q,\omega = ct)$ will develop at $Q_p/2$. On the other hand, a rather different behaviour is observed for the crystal where, at low energy transfers, only intensities arising from the strong Bragg reflections are seen and a behaviour which approaches $Q^2S(Q,0)$ is revealed for large energy transfers. A quantitative comparison between the inelastic structure factors derived from simulational and experimental means becomes difficult since the required high energy resolution implies a low incident energy, thus severely restricting the available kinematic range, and on the other hand, resolution-broadening effects complicate the removal of the elastic contribution at low energy transfers. Even so, the inelastic intensities corresponding to the elastic, 0.5 THz and 1 THz energy transfers (the only significant region accessible experimentally) derived from the high-resolution experiment are shown in figure 8. As can be seen, the 0.5 THz data show for wavevectors below 1 Å^{-1} a rather different behaviour to that shown by the curve corresponding to 1 THz, which can be ascribed to the rise seen in the simulation data becoming more prominent for Q values below 0.5 Å^{-1} (see figure 7). Such an increase in intensities should not be due to multiple-scattering effects since, as shown by the elastic component, these contributions have been taken care of. A remnant of the elastic peak is also seen in the 0.5 THz profile. On the other hand, the curve for 1 THz transfer shows the increasing contribution of the higher-Q excitations as well as a

small hump at about $Q_p/2$, which seems related to the small feature also appearing in the former spectra, and may be an indication of the feature seen in the MD data displayed in figure 7 for large energy transfers, although it becomes difficult to ascertain its reliability since the neutron kinematics does not allow the exploration of smaller momentum transfers. In this respect, the comparison between MD and experiment for higher energy transfers is precluded for the very same reason, and a significant comparison of some previous data [9] measured under far worse resolution with the MD results is hindered by the rather low counting statistics of the former.

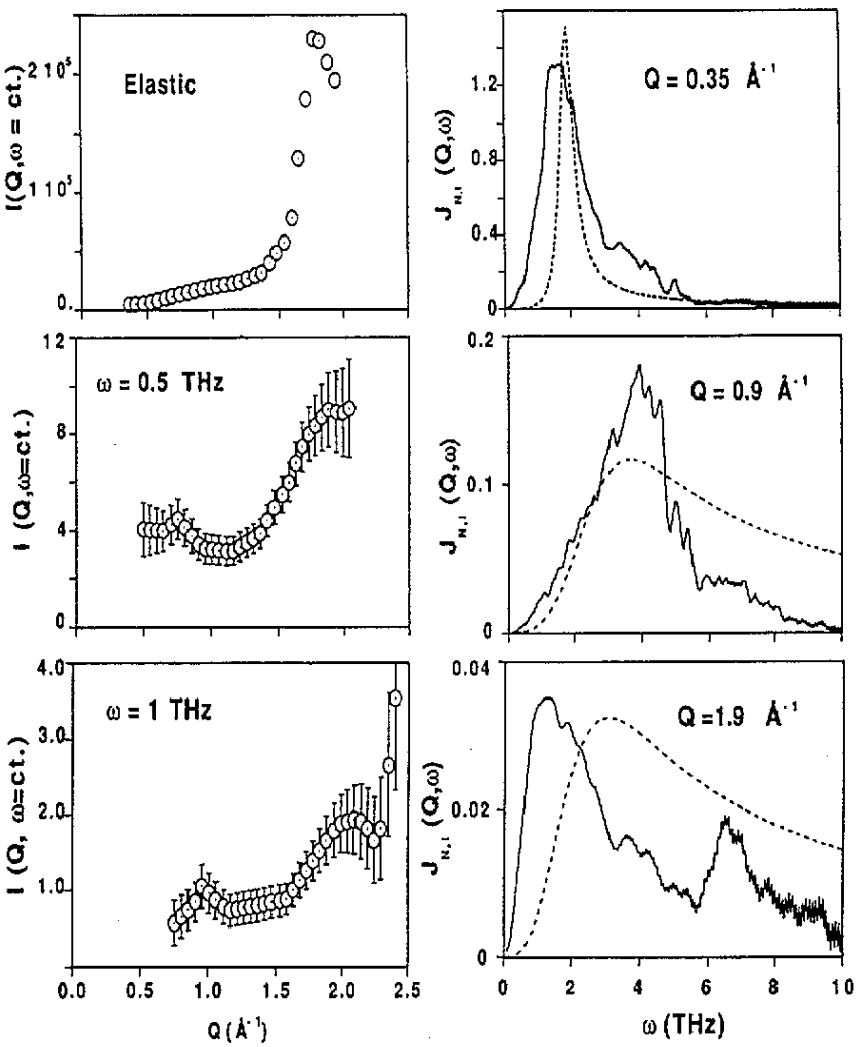

Figure 8. The left column shows the wavevector dependence of the intensities of the high-resolution experiment (IN6) for the elastic line (top) and for two energy transfers with the values given. The units for the abscissae are counts after normalization to a vanadium standard. The right-hand side shows a comparison of $J_{N,I}(Q,\omega)$ longitudinal current correlations as calculated from the MD simulation (full curve) and those calculated using the parameter sets employed for the analysis of the high-incident-energy data (see text).

4.3. Average excitation frequencies

From what is known for the coherent neutron scattering response of polycrystals, and as has also been evidenced in the present work, once a polycrystalline average is performed only excitations below the Brillouin zone centre remain as relatively well defined entities, even if the observable quantities are now envelopes over the individual lattice modes. Above $Q_p/2$ the presence of higher-lying excitations will substantially complicate the analysis of experimental data, since more than one oscillator function in (1) will be required to adequately model the data. An average or effective frequency ω_m corresponding to the frequency maxima of $J_{N,l}(Q,\omega)$ seems a more adequate tool to characterize the observed mode envelopes than the lowest-frequency moments of the scattering law, and for the lowest-lying (acoustic) excitations such frequencies should become comparable in the hydrodynamic limit with an average sound velocity (the frequencies ω_m corresponding to peaks in the current–current correlations are formally the same as the renormalized phonon frequencies $\Omega = \sqrt{\omega_q^2 + \Gamma_q^2}$ as used in (1). Some discussion regarding the physical meaning of these frequencies is given in [21].)

A comparison between experimental frequencies and their simulation counterparts shown in figure 3 clearly evidences the need to account for both the low-frequency ($\omega_m \simeq 0.5$ THz) feature seen in the high-resolution experiment and the higher-lying optic branches ($\omega_m \simeq 3.6$ THz) for momentum transfers above $\sim Q_p/2 = 0.9\,\text{Å}^{-1}$, if the simulation results are to be reproduced. An illustration of the origin of such a discrepancy can be seen in figure 8, where $J_{N,l}(Q,\omega)$ functions from the MD calculations are compared with those calculated for a damped harmonic oscillator with the same parameters used to fit the experimental intensities [8]. Notice that the ω_m frequencies derived from experiment are now the peak maxima of the broken curves shown in the figure. As can be clearly seen, approximating the experimental spectra by only one inelastic component is a fair approximation up to $Q_p/2$ (the rather small width of the experimental curve for $Q = 0.35\,\text{Å}^{-1}$ is due to the limited kinematic range available at these wavevectors), whereas an ω_m frequency which is a weighted average of those corresponding to peaks at 1.5 THz, 3.8 THz and 7 THz was extracted from the experiment (analysed well before the simulation data became available). A comparison between experimental and simulated spectra can thus be regarded as semiquantitative, mainly because of the scarce data measured so far (for a comparison of figure 8 with experimental data as measured, see figure 2).

The close similarity of the width of both polycrystalline and glassy spectra at the lowest explored wavevectors seems to be in qualitative agreement with some theoretical predictions based upon effective medium approaches [1], where a no- or low-damping regime was found below a certain cutoff frequency. Such a frequency can be correlated with that where the $Z(\omega)$ density of states starts to deviate strongly from the Debye behaviour, which in our case is located at about 0.1 THz [6], and therefore it becomes difficult to test such a correlation since measurements at too small wavevectors are then required. In any case, the crucial problem of separating those contributions to the linewidth arising from the continuous distribution of force constants from the ones due to finite-lifetime effects must be addressed before any quantitative comparison of the damping ratios can be carried out.

4.4. Low-frequency inelastic scattering

From a comparison of the present experimental data with those analysed for an incoherent scattering sample [6,7], as well as from an analysis of the low-temperature specific heat from the integrals of the $Z(\omega)$ vibrational densities of states derived from experiment and

MD simulation, it is clear that the low-frequency feature appearing at about 0.5 THz can be identified with the so-called boson peak, common (but not universal) to a large number of glasses.

A comparison of polycrystal and glass spectra, particularly at Q values of about Q_p given in figure 6, shows that a correlate of the excitations characteristic of the glass can also be found at higher frequencies in the polycrystal. In the latter case such a feature originates from the lowest-lying librational–translational peaks present in $Z(\omega)$ (the mode eigenvectors are given in table 2 of [6]), and the close similarity in the shapes of both crystal and glass peaks strongly suggests some common microscopic origins. In fact, most of the glasses studied at this level of microscopic detail [3, 20] have evidenced the strong harmonic librational–translational character of these low-frequency peaks, and the available evidence for this glass [6, 7] as well as for glassy selenium at moderately low temperatures [22] indicates that a coarse-grained description in terms of the $Z_{com}(\omega)$, that is, the density of states projected into the molecular centres of mass, should suffice to account for the thermal anomalies at intermediate temperatures. The specific mechanism by means of which these low-frequency librations couple to the strain fields causing a softening of the elastic constants still has to be elucidated, and further simulational efforts in this direction seem worth attempting.

5. Conclusions

Up to the present moment, a rather limited number of glasses have been studied using an approach similar to that followed in the present work; in particular, no real system has been discussed in terms of the lineshape characteristics of the measured $S(Q, \omega)$ dynamic structure factors, although some preliminary results on metallic glasses are now emerging (results for a ternary metallic glass have been discussed by Dahlborg and co-workers [23]. In such a case additional complications appear due to the substantial contribution of inelastic magnetic intensities. Data for a binary glassy alloy are given by Suck and co-workers [23] although no analysis of the lineshapes was attempted.)

From the data shown above, it becomes clear that at least for wavevectors up to half the maximum of the static structure peak Q_p, the experimental or simulated glass spectra can be described in terms of an average frequency ω_m which is readily obtainable from experiment as that corresponding to the most prominent maxima of the function $J_{N,I}(Q, \omega)$. The physical soundness of such a magnitude has been evidenced, as it leads to the correct thermodynamic limit. Above such a limiting wavevector, a number of finite-frequency features will appear which are strongly reminiscent of those appearing in the generalized vibrational densities of states and are strongly sample dependent, the origin of which can be best investigated from an analysis of the mode eigenvectors of the corresponding polycrystal as exemplified in [6]. On the other hand, the characteristic (0.5 THz) low-frequency feature clearly noticeable in the spectra of the incoherently scattering sample [6, 7] will introduce an additional complication if a full lineshape analysis is attempted. A significant dependence on the wavevector was found in the present case [9] as well as in the pioneering study of [24] for a metallic glass, something which provides evidence for its strongly collective character, a fact apparently unnoticed to date.

Even if a fully quantitative comparison beyond that regarding the average frequencies between simulated and experimental spectra seems to be precluded by a number of experimental difficulties, as well as from the inherent simplifications of the model potentials used, the concurrent use of both techniques allows an unambiguous identification of the most relevant features appearing in the inelastic spectra.

Finally, the approach followed in this paper will enable us in future to go beyond the phenomenological treatments of the low-frequency (boson) peaks which currently pervade the literature and find their microscopic origins.

Acknowledgments

The MD calculations were carried out at the ISIS Science Division at RAL; thanks are given for the allocation of the necessary computational resources. This work has been supported in part by DGICYT grant No PB92-0114-C03.

References

[1] Schirmacher W and Wagener M 1992 *Phil. Mag.* **65** 607
[2] Buchenau U, Galperin Yu M, Gurevich V L, Parshin D A, Ramos M A and Schober H R 1992 *Phys. Rev.* B **46** 2798
[3] Sethna J P, Grannan E R and Randeria M 1991 *Physica* B **169** 316
Grannan E R, Randeria M and Sethna J P 1988 *Phys. Rev. Lett.* **60** 1402; 1990 *Phys. Rev.* B **41** 7784, 7799
[4] Hunklinger S 1987 *Heidelberg Coll. on Glassy Dynamics* ed J L van Hemmen and I Morgenstern (Berlin: Springer) p 94
[5] Cahill D G and Pohl R O 1988 *Ann. Rev. Phys. Chem.* **39** 93
Pohl R O 1981 *Amorphous Solids. Low Temperature Properties* ed W A Phillips (Berlin: Springer) p 27
[6] Bermejo F J, Alonso J, Criado A, Mompean F J, Martinez J L and Garcia-Hernandez M 1992 *Phys. Rev.* B **46** 6173
[7] Garcia-Hernandez M, Burriel R, Bermejo F J, Pique C and Martinez J L 1992 *J. Phys.: Condens. Matter* **4** 9581
[8] Bermejo F J, Martin D, Martinez J L, Batallan F, Garcia-Hernandez M and Mompean F J 1990 *Phys. Lett.* **150A** 201
[9] Bermejo F J, Martinez J L, Garcia-Hernandez M, Martin D, Mompean F J, Alonso J and Howells W S 1991 *Europhys. Lett.* **15** 509
[10] Carlson H G and Westrum E F 1971 *J. Chem. Phys.* **54** 1464
[11] Johnson M W 1974 *AERE Report* 7682
[12] Alonso J, Bermejo F J, García-Hernández M, Martínez J L and Howells W S 1991 *J. Mol. Struct.* **250** 147
Alonso J, Bermejo F J, Garcia-Hernandez M, Martinez J L, Criado A and Howells W S 1992 *J. Chem. Phys.* **96** 7696
[13] Torrie B H, Weng S X and Powell B M 1989 *Mol. Phys.* **67** 575
[14] Anderson A, Andrews B, Meiering E M and Torrie B H 1988 *J. Raman Spectrosc.* **19** 85
[15] Steytler D C, Dore J C and Montague D C 1985 *J. Non-Cryst. Solids* **74** 303
[16] Bermejo F J, Ramírez R, Martínez J L, Prieto C, Batallán F and García-Hernández M 1991 *J. Phys.: Condens. Matter* **3** 569
[17] Bathia A B and Singh R N 1986 *Mechanics of Deformable Media* (Bristol: Hilger) p 94
Hirth J P and Lothe J 1968 *Theory of Dislocations* (New York: Wiley)
[18] Grest G S, Nagel S R and Rahman A 1984 *Phys. Rev.* B **29** 5968
[19] Nagel S R, Grest G S, Feng S and Schwartz L M 1986 *Phys. Rev.* B **34** 8667
[20] Buchenau U, Prager M, Nucker N, Dianoux A J, Ahmad N and Phillips W A 1986 *Phys. Rev.* B **34** 5665
[21] Dorner B 1992 *Physica* B **180–1** 265
[22] Garcia-Hernandez M, Bermejo F J, Fåk B, Martinez J L, Enciso E, Almarza N G and Criado A 1993 *Phys. Rev.* B **48** 149
[23] Dahlborg U *et al* 1993 *Proc. Workshop on Dynamics of Disordered Materials II (Grenoble, 1993)*
Suck J B, Egelstaff P A, Robinson R A, Sivia D S and Taylor A D 1992 *Europhys. Lett.* **19** 207
[24] Suck J B, Rudin H, Guntherodt H L and Beck H 1983 *Phys. Rev. Lett.* **50** 49